



HAL
open science

Quantifying silo flow using MRI velocimetry for testing granular flow models

Luke Fullard, Daniel J. Holland, Petrik Galvosas, Clive Davies, Pierre-Yves Lagrée, Stéphane Popinet

► **To cite this version:**

Luke Fullard, Daniel J. Holland, Petrik Galvosas, Clive Davies, Pierre-Yves Lagrée, et al.. Quantifying silo flow using MRI velocimetry for testing granular flow models. *Physical Review Fluids*, 2019. hal-02164393

HAL Id: hal-02164393

<https://hal.science/hal-02164393>

Submitted on 25 Jun 2019

HAL is a multi-disciplinary open access archive for the deposit and dissemination of scientific research documents, whether they are published or not. The documents may come from teaching and research institutions in France or abroad, or from public or private research centers.

L'archive ouverte pluridisciplinaire **HAL**, est destinée au dépôt et à la diffusion de documents scientifiques de niveau recherche, publiés ou non, émanant des établissements d'enseignement et de recherche français ou étrangers, des laboratoires publics ou privés.

Quantifying silo flow using MRI velocimetry for testing granular flow models

Luke Fullard*

*School of Fundamental Sciences,
Massey University, New Zealand.*

Daniel J. Holland

*Department of Chemical and Process Engineering,
University of Canterbury, New Zealand.*

Petrik Galvosas

*School of Chemical and Physical Sciences,
Victoria University, New Zealand*

Clive Davies

*School of Food and Advanced Technology,
Massey University, New Zealand.*

Pierre-Yves Lagrée, Stéphane Popinet

*Institut Jean le Rond d'Alembert,
CNRS UMR 7190
Sorbonne Université,
Paris, France.*

(Dated: June 21, 2019)

In this work we present experimental results of the gravity-driven discharge of poppy seeds from 3D-printed silos. The velocity fields of the flowing poppy seeds are measured using Magnetic Resonance Imaging (MRI) velocimetry techniques. Crucially, this approach allows the velocity field to be determined throughout the flow domain, unlike visual techniques such as Particle Image Velocimetry (PIV) and related methods where only the flow at or near the wall is accessible. We perform the experiment three times; with 3D-printed silos of cone half angles 30° and 50° respectively, and then repeat the 30° silo experiment, but with a layer of poppy seeds glued to the silo wall to create a “rough wall” condition. In our experiments, we observe and quantify velocity fields for three well known granular flow regimes; mass flow, funnel flow, and rat-holing. The results of the experiments are compared to equivalent output of numerical simulations. In this mathematical model, the well-known $\mu(I)$ friction law is used to define an effective granular viscosity, and the flow is solved using a standard Navier-Stokes type solver. While the results are generally encouraging, it is noted that some aspects of the model are lacking and should be improved; in particular, the rat-holing effect observed in one of the MRI experiments was not predicted by the model, nor was the exact volumetric flow rate from any of the silos. Suggestions for model improvement are discussed.

I. BACKGROUND AND INTRODUCTION

Granular matter is well known to behave in complex and often unexpected ways. Particles in a granular assembly may act in a solid-like, liquid-like, or gas-like manner, with the transition between these phases often difficult to

* L.Fullard@Massey.ac.nz

define and quantify [1]. A commonly studied granular system is gravity-driven silo discharge. In addition to being a system of great practical importance, silo flow can also display a variety of interesting flow dynamics. Depending on the design of the silo (i.e. the silo half angle, the friction between particles, the friction between the silo walls and particles, and the size and shape of the particles), the flow may be either mass-flow, funnel flow, or display rat-holing [2, 3]. In mass flow, all particles in the silo are in motion with no stagnant zones; in funnel-flow there are regions within the silo where particles flow, but there are also stagnant regions (and an interface between flowing/stagnant regions); when a silo displays rat-holing, flow only occurs in a central core approximately the size of the silo opening, with large stagnant regions surrounding this core. Rat-holing can be considered an extreme case of funnel flow, but the flow is often observed to be intermittent and transient, whereas in a general funnel flow the dynamics are much more steady. Due to the variety of flow regimes, the silo provides an excellent test of numerical models of granular dynamics.

Apart from testing numerical codes, quantifying velocity fields in the silo is of great industrial importance, for example, in the study of particle mixing and segregation as particle blends are discharged from a silo. While there have been many Discrete Element Modelling (DEM) [4–6] and continuum models [7–14] developed to study the silo, experimental measurements and validations are still required.

The vast majority of experimental characterisation of the velocity vector field in a discharging silo has been using visual imaging methods in transparent silos (both conical and planar). Techniques such as Particle Image Velocimetry (PIV) and Particle Tracking Velocimetry (PTV) have been successfully applied to measure the grain velocity *at the silo walls* [15–20]. On the contrary however, experimental measurements of velocity fields away from silo walls (i.e. in the bulk of the flow) are particularly difficult to obtain. Previous attempts to experimentally quantify 3D velocity fields in silos

have included X-ray CT [21, 22], timing tracer discharge [23], Scanning gamma ray tomography [24, 25], and single profile proton absorptiometry [26], however, all of these methods give limited velocity profile information, and usually provide averaged data, data at discrete points, or data along a line only, rather than on a plane.

Magnetic Resonance Imaging (MRI) is an alternative technique that can study flow in optically opaque systems. MRI has been applied to non-silo granular systems [27–34] to quantify parameters such as velocity fields and packing. Kawaguchi [35] observed the flow type, either mass or funnel flow, in silos using tagged MR imaging. In this approach, bands of particles are tagged at one point in time and then the positions of these tagged particles imaged after a defined delay (in this case 100 ms). The deformation of the tagged layers was observed visually. In theory this technique could be extended to estimate the velocity in a silo using further image processing techniques, but this would give only an indirect measure of the velocity fields. MRI has also been used to obtain the only reported direct, quantitative measurement of the silo velocity data on a plane away from the silo walls that we have found [36], though the range of silo flow conditions studied was limited. The first objective of the current article is to extend the work of Gentzler and Tardos [36] to obtain velocity field data for a wider range of silo flow situations. Firstly, we report on both the vertical and horizontal component of the velocity at the outlet. Secondly, we also measure particles of a large diameter ($\approx 1\text{ mm}$) such that the effect of the surrounding air on the particle dynamics near the orifice is not significant [37]. Thirdly, we consider the effect of changing the hopper geometry. Finally, we consider the effect of rough-walls on the particle dynamics. These last two aspects of the experiment mean that flow is studied across the three major flow regimes observed in silos.

A second objective is to assess the applicability of the so-called $\mu(I)$ friction law [38] for reproducing the velocity fields which we experimentally measure. Previously, the $\mu(I)$ friction law has been used to define an effective gran-

139 ular viscosity for use in incompressible contin-
 140 uum flow models. Such an approach has been
 141 successfully applied to the granular column col-
 142 lapse and to some silo flows. [7, 8, 13, 39].
 143 However, the velocity fields produced by the
 144 model have not been rigorously tested against
 145 experimental data. In particular, we examine
 146 the model applicability to reproduce the three
 147 silo flow modes, mass flow, funnel flow, and rat-
 148 holing, which we observe in our experimental
 149 results.

150 II. MATERIALS AND METHODS

151 1. Particle properties

152 In this study, poppy seeds were chosen as the
 153 granular material of interest due to their par-
 154 ticle size, their price and availability, and the
 155 fact that they contain abundant free oil which
 156 allows a strong signal to be detected by the
 157 MRI equipment. The poppy seeds were non-
 158 spherical, and were kidney shaped, as seen in
 159 Figure 1. The poppy long diameter was ap-
 160 proximately 1.25 mm , while the short diameter
 162 was approximately 0.85 mm . A standard sieve
 163 experiment was performed and $\approx 93\%$ of the
 164 particles were found to be between $710\ \mu\text{m}$ and
 165 $1180\ \mu\text{m}$, with a Sauter mean diameter [40], d ,
 166 of $951\ \mu\text{m}$.

167 2. Silo system design

168 The silo feeding system was designed to the
 169 specifications of the bore of the MRI apparatus
 170 in such a way that the poppy seeds were fully
 171 contained and never came in direct contact with
 172 the MRI apparatus itself. A system of perspex
 173 pipes of decreasing diameter was used to feed
 174 the poppy seeds into the test silo (the region
 175 to be imaged by the MRI) and then out of the
 176 bottom of the system. These pipes were con-
 177 nected using a series of push-fittings with small
 178 tolerances. Figure 2 A. displays the full system
 179 of pipes and the test silo, while B. is a close-
 180 up of the silo itself. The silo was designed in

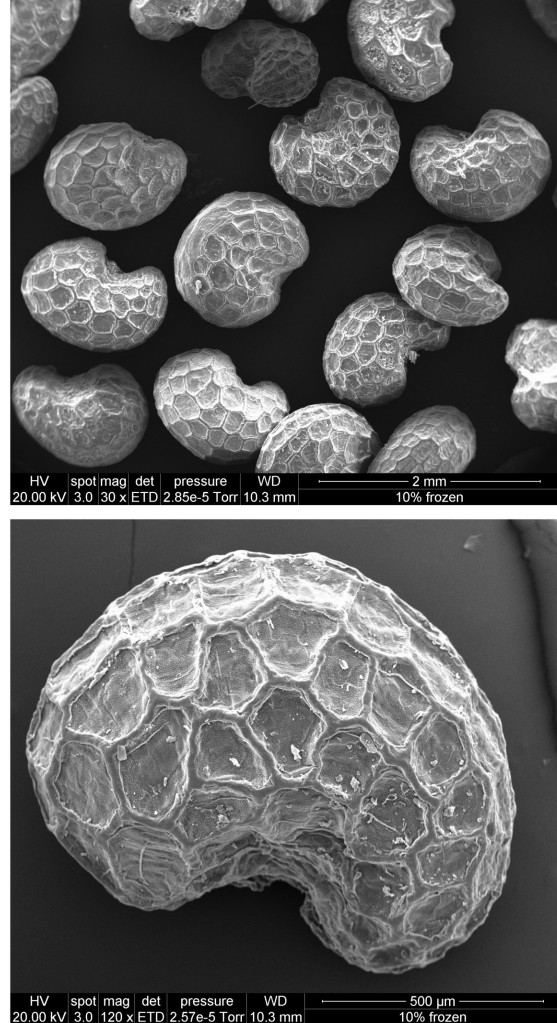


FIG. 1. Scanning Electron Microscope images of a sample of poppy seeds. It is apparent from the image that the seeds are non-spherical with a kidney shape. The surface of the seeds is also seen to be textured. A scale is included at the bottom of each image. **A.** An image of multiple poppy seeds. **B.** A close up of a single poppy seed.

a CAD program, 3D printed from ABS plastic, and the opening at the bottom of the silo, D_0 , was drilled to a diameter of 6.5 mm (note that this is ≈ 6.5 times greater than the Sauter mean diameter, d , of the particles to avoid jamming

186 [18, 41]). The inner diameter of the silo, W ,
 187 was 23.5 mm . Since $D_0 > 6.5d$, $W > 2.5D_0$,
 188 and the bed height is always deeper than the
 189 silo opening diameter, the flow rate from the
 190 silo can be expected to be independent of the
 191 silo geometry. [42] The silo half angle, ϕ , was
 192 changed between each experiment; the first silo
 193 had a 30° half angle, the second 50° , and the
 194 third was another 30° half angled silo but with
 195 rough walls. The rough walled silo was printed
 196 in two halves, then poppy seeds were glued onto
 197 the inner silo walls in a single layer, and finally,
 198 the two halves were glued together to form a
 199 full silo. We note that the diameter of the final
 200 pipe, labeled pipe 3 in Figure 2, was wider than
 201 the silo opening. This design was to avoid the
 202 well-known standpipe flow rate effect [43] which
 203 does not occur unless the pipe below the silo is
 204 full [43]. Since the silo opening diameter was
 205 smaller than the exit pipe this was not the case
 206 and the standpipe effect was avoided.

3. Experimental method

A Bruker Avance I Nuclear Magnetic Resonance spectrometer with a 9.4 T wide bore magnet located at Victoria University of Wellington, New Zealand was used for the experiments. A 30 mm diameter radio-frequency coil was used for excitation and detection. A three-axis shielded Micro2.5 gradient set capable of producing a maximum gradient strength of 1.51 T m^{-1} was used for imaging and flow encoding. The pipes and silo were connected together and carefully inserted into the MRI. The silo and upper two pipes were filled from above through a funnel. A bucket was placed under the system to collect the discharged particles. As the particles were discharged the system was periodically refilled from above such that the upper pipe (pipe #1) was never more than half empty. Note that the flow rate from the silo was constant and independent of fill height as is implicit in the Beverloo flow rate equation [44, 45].

The vertical (i.e. in the axial direction) and horizontal (i.e. in the radial direction) components of velocity of the poppy seeds were measured using a phase encoded velocity imaging sequence [46]. The image was obtained using a spin echo acquisition with a slice selective refocussing pulse. To enable accurate measurements of the wide range of velocities present in the system, experiments were repeated with 8 flow encoding gradients. The velocity was calculated from a linear fit to as many of these data points as possible. For the fastest flowing regions, typically only three experiments with the weakest flow encoding gradients were used, while in the slow moving regions all 8 experiments were used. The gradient encoding duration δ was set to 0.7 ms , the observation time was 2.5 ms , and the maximum gradient strength was set to 0.07 T m^{-1} in the vertical direction and 0.14 T m^{-1} in the horizontal direction. These settings gave a maximum field of flow of approximately 2 m s^{-1} with a minimum detectable velocity of $1 \times 10^{-3} \text{ m s}^{-1}$,

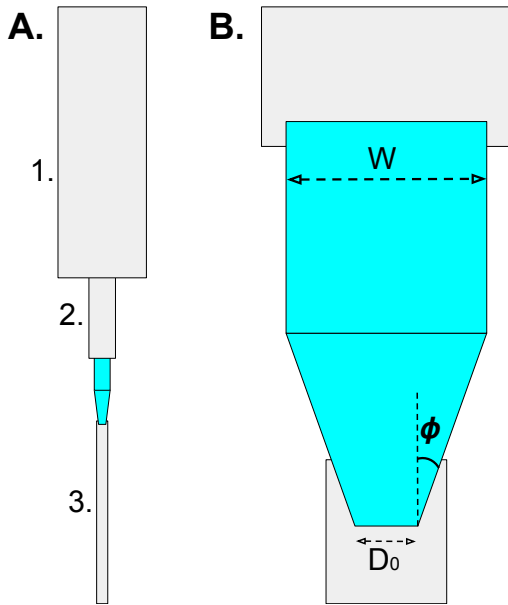


FIG. 2. A sketch of the piping and silo in the experimental set-up (not to scale).

A. The system is loaded from above. the seeds flow through the largest pipe #1. into the more narrow pipe #2. through the test silo section, and out through pipe #3. **B.** A close up of the test silo section.

where the minimum detectable velocity corresponds to a signal-to-noise ratio of 2. Images were acquired at a spatial resolution of 0.45 mm in the horizontal direction and 1.18 mm in the vertical direction with a slice thickness of 1 mm . The total acquisition time for the images was approximately 50 minutes. Flow-encoded NMR images can acquire a phase arising from the imaging gradients themselves. It is common practice to correct this phase by acquiring measurements on a static sample. Here images of a static bed were also acquired. The phase change for these was negligible, thus no correction was required.

Three MRI experiments were performed, one with a silo of 30° half angle, one with a silo of 50° half angle, and finally with another silo of 30° half angle, but with rough walls (with particles glued on the silo walls).

4. Numerical model

One goal of this work is to model the silo using a continuum model of granular flow. Recently, the $\mu(I)$ law for the friction of granular materials has been used to define an effective viscosity in granular flow simulations. This viscosity was successfully implemented into an incompressible Navier-Stokes solver (Gerris Flow Solver [47]) to model dense granular flow in a variety of situations [7, 8, 13, 39]. For our situation, an axisymmetric domain was used so that our 3D silo could be modelled in 2D. The governing equations of incompressible flow were solved in Gerris;

$$\nabla \cdot \mathbf{u} = 0, \quad (1)$$

$$\rho \left(\frac{\partial \mathbf{u}}{\partial t} + \mathbf{u} \cdot \nabla \mathbf{u} \right) = -\nabla p + \nabla \cdot (2\eta \mathbf{D}) + \rho \mathbf{g}$$

In the above continuity and momentum equations, \mathbf{u} is the velocity vector, ρ the flowing (bulk) density, p the local isotropic pressure, η the effective (or apparent) granular viscosity, and \mathbf{D} the rate of strain tensor. The effective viscosity is defined as

$$\eta_{eff} = \frac{\mu(I)p}{D_2}, \quad (3)$$

but in practice a regularised effective viscosity was used to avoid infinite values when the fluid is experiencing small shear;

$$\eta = \min \left(\frac{\mu(I)p}{D_2}, \eta_{max} \right). \quad (4)$$

Here, $D_2 = \sqrt{\frac{1}{2} D_{ij} D_{ij}}$ is the second invariant of the strain rate tensor, where $D_{ij} = \frac{\partial u_i}{\partial x_j} + \frac{\partial u_j}{\partial x_i}$, and $\mu(I)$ is the granular friction law;

$$\mu(I) = \mu_1 + \frac{\mu_2 - \mu_1}{I_0/I + 1}, \quad (5)$$

with μ_1 , μ_2 , and I_0 parameters. The variable I is the granular inertial number and is defined as

$$I = \frac{d D_2 \sqrt{\rho_p}}{\sqrt{p}}, \quad (6)$$

where d is the particle diameter and ρ_p is the solid particle density.

In our axisymmetric numerical model we apply no-slip conditions on both of the velocity components at the silo walls, a symmetry condition along the axis of symmetry, homogeneous Neumann velocity boundary conditions (for each velocity component) at the top and bottom of the silo, and we set $p = 0$ at the top and bottom of the silo. Note that other boundary conditions could be used at the silo wall (for example, to allow slip at the silo wall [48, 49]), but the effect of more complex boundary conditions is left for future work. For the 30° silo with rough walls, the simulation domain was reduced by a particle diameter in size to account for the reduced dimensions due to the layer of particles glued to the silo walls, but the silo opening was kept at 6.5 mm . No other change to the boundary conditions was made.

Parameters used in our simulation are listed in table I. The first friction parameter, μ_1 , was chosen based on measurements of the angle of repose of the poppy seeds which was found to be approximately 31° , hence, $\mu_1 = \tan 31 = 0.6$. The upper limit on the friction angle, defined by parameter $\tan^{-1}(\mu_2)$, was expected to be

around 60° since our MRI experimental results for the velocity in the 30° silo (to be presented in Figure 3) showed small slow/stagnant regions at the transition from the conical to cylindrical section. We also noted that larger values of I_0 kept the incompressible $\mu(I)$ model in the well-posed regime for a wider range of inertial numbers than for low values of I_0 [50]. For this reason, various values of $\tan^{-1}(\mu_2) \approx 60^\circ$ and I_0 between 0.05 and 1 were tested. It was found that the parameters $\mu_2 = 1.7$ and $I_0 = 0.5$ gave a good match to experimental data (to be discussed), gave a wide range of well-posed inertial number values, and, importantly, were physically realistic.

TABLE I: Parameters used in the numerical model.

Name	Symbol	Unit	Value
Bulk density	ρ	kg/m^3	600
Particle density	ρ_p	kg/m^3	1000
Particle diameter	d	mm	0.951
Friction coefficient #1	μ_1	-	0.6
Friction coefficient #2	μ_2	-	1.7
Reference inertial number	I_0	-	0.5

III. RESULTS

1. MRI Experimental Results

The results of the phase encoded velocity imaging sequence experiment were converted into a Matlab data file and plotted as a contour map. In Figure 3 the logarithm of the vertical component of velocity is plotted for each of the three silos, where $\mathbf{u} = (u, v)$ is the velocity vector with u, v the horizontal and vertical velocity components respectively. The logarithm of the magnitude of the horizontal component of velocity (u) is shown in Figure 4. The lighter (yellow) regions are zones of rapid flow, while the darker (purple/blue) regions indicate slow or stagnant flow. Horizontal velocity measurements were not available for the 30° silo with rough walls because the magnitude of the horizontal component of velocity was very small and

was of the same order as the noise in the experiment.

The most immediate observation from Figure 3 is that for each silo we have a different flow regime. In the 30° silo we observe mass flow. The particles in the silo at every location are in motion, with a possible small exception at the transition from the cone to the cylindrical section. In the 50° silo we observe funnel flow. There is a region of flow in the center of the silo and this region of flowing material widens as we move further up into the silo. There is a clear stagnant region of flow that surrounds the flowing particles. This stagnant region shrinks as we transition higher into the silo. In the 30° silo with rough walls (i.e. with a layer of poppy seeds glued to the wall) we observe the rat-holing effect. There is a fast core (roughly the diameter of the silo opening) of flowing particles surrounded by a region of stagnant material. The size of this stagnant zone does not perceptibly change as we transition higher into the silo. It is also apparent that the velocity field in the flowing zone remains continuous as we move higher in the silo, past the transition from the conical to cylindrical section (i.e. we do not observe velocity discontinuities or shocks). This is in contrast to predictions from Mohr-Coulomb plasticity based models [2, 51].

In order to assess the appropriateness of the incompressible assumption in our numerical model, we quantify the volumetric flow rate as a function of height above the silo opening. For each MRI experiment we use the vertical component of velocity (v) to calculate the volumetric flow rate;

$$Q(z) = 2\pi \int_{r(z)=0}^{r(z)=R(z)} v r dr, \quad (7)$$

where $r(z)$ is the radial coordinate from the axis of the silo, and $R(z)$ is the radius of the silo at height z above the opening. The resulting flow rates for each experiment are plotted in Figure 5.

It is apparent from the figure that the volumetric flow rate is approximately constant throughout the silo in the 30° silo, but this is not so for the 50° and 30° silo with roughened

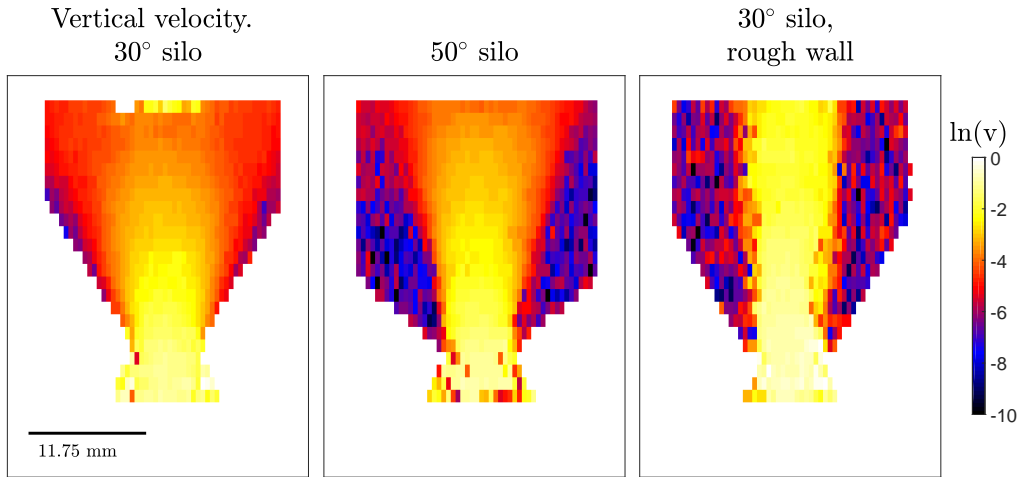


FIG. 3. The log of the magnitude of the vertical component of velocity (v) is plotted for each of the three silos. Mass flow is observed in the 30° silo, funnel flow in the 50° , and rat-holing in the 30° silo with rough walls (with particles glued to the silo wall). Yellow regions indicate rapid flow, while purple/blue areas indicate slow to stagnant zones.

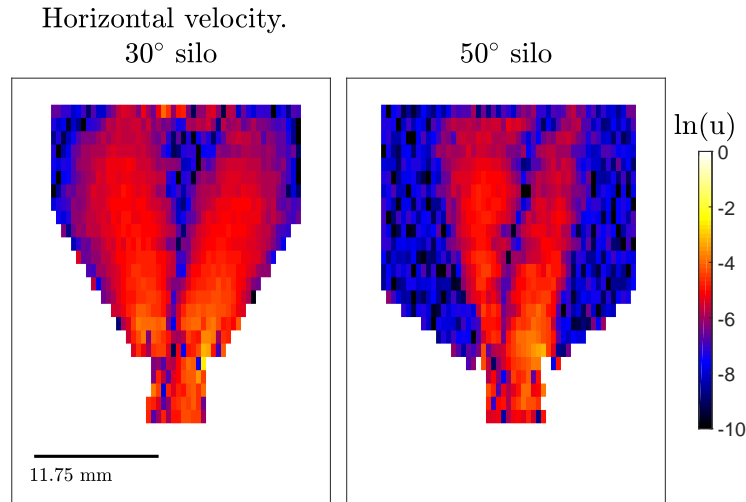


FIG. 4. The log of the magnitude of the horizontal component of velocity (u) for the 30° and 50° silos.

414 walls. In these two non-constant flow rate cases, ⁴²⁰
 415 the volumetric flow rate $Q(z)$ is seen to be $\approx 2 \times$ ⁴²¹
 416 higher near the opening than it is in the bulk of ⁴²²
 417 the silo. This variation in flow rate could arise ⁴²³
 418 either from a measurement error or a dilation ⁴²⁴
 419 of the flow at the outlet. The signal intensity ⁴²⁵

at the outlet in all three images is less than half
 that in the bulk, which would be consistent with
 a dilation of the flow at the outlet. However,
 in these measurements there is also significant
 attenuation of the signal due to the motion of
 the particles, so the images are not quantitative

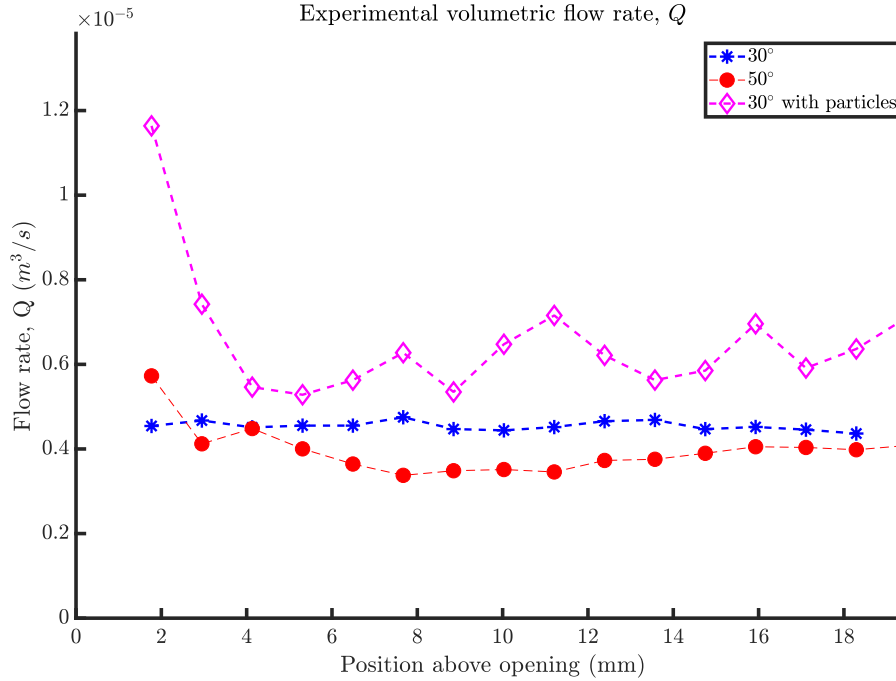


FIG. 5. The volumetric flow rate, $Q(z)$, for each of the three silo experiments as a function of height above the silo opening.

in solid fraction. Therefore it is important to consider the errors that arise in measurement of velocity. MRI measurements of the velocity are prone to error in regions of high velocity but this error will tend to cause an underestimation of the velocity as faster moving particles are more heavily attenuated than slower moving particles. The flow rate is seen to increase towards the outlet, hence, it is unlikely that a velocity measurement error could explain the observed flow rate variation. Therefore, it is concluded that, for the funnel flow and rat-holing silos, there is significant dilation of the flow near the opening, and the assumption of incompressibility is likely to be erroneous, at least near the silo opening. In a similar system, a wedge shaped hopper, a significant reduction in bulk density has been observed [52]. As a point of context, in the numerical model the incompressibility condition is enforced (up to a tolerance) and it was found that the change in the volumetric

flow rate was less than 1% throughout the silo. Here we assume that the use of an incompressible flow model has only a small effect on the predicted velocity fields, since in the bulk of the silo the flow rate is relatively constant, changing only near the silo opening. However, the dilation near the opening will change the predicted flow rate values. Given this result and model assumption, when comparing experimental and numerical results with an incompressible flow assumption, the velocity should be adjusted to account for the change in volumetric flow rate. In practice this is achieved by normalising the velocity by the volumetric flow rate at each local height above the silo opening. Furthermore, we quantified the mass flow rate, \dot{m} , from each of the silos by measuring the mass ejected from the system in a given time. For the 30° silo we found $\dot{m}_{30} = 2.11 \pm 0.07$ g/s, for the 50° silo, $\dot{m}_{50} = 1.74 \pm 0.09$ g/s, and for the 30° silo with particles on the wall,

468 $\dot{m}_{30}^p = 2.2 \pm 0.1 \text{ g/s}$. The reduction of the 512
 469 mass flow rate between the 30° and 50° silos 513
 470 is compared with corrections made to the Bev-514
 471 erloo flow rate to account for hopper half angle 515
 472 [53]. Assuming that the Beverloo parameters 516
 473 and bulk density is equal between the two silos 517
 474 of differing half angles, the ratio of the two flow 518
 475 rates is given as $M = \frac{f(50^\circ)}{f(30^\circ)}$, where the func-519
 476 tion $f(\alpha) = \sqrt{\frac{1-\cos \alpha}{2 \sin^3 \alpha}}$. The theoretical ratio M 520
 477 is calculated as 0.86, while the experimental ra-522
 478 tio in our system, $\frac{\dot{m}_{50}}{\dot{m}_{30}}$ is found to be 0.82 ± 0.05 , 523
 479 in good agreement with the theoretical value. 524

480 2. Numerical Model Results: 30° silo 527

481 To directly compare the $\mu(I)$ numerical re-529
 482 sults to the MRI experimental results a results 530
 483 file was imported from Gerris into Matlab which 531
 484 contained vertical and horizontal components of 532
 485 velocity. This data was interpolated onto five 533
 486 horizontal lines which correspond to the loca-534
 487 tions of measurements taken in the MRI exper-
 488 iments. Thus, the horizontal and vertical com-
 489 ponents of velocity predicted in the model could 535
 490 be directly compared to the experimental data.

491 As previously mentioned, the volumetric flow 536
 492 rate in the silo experiments was not a constant 537
 493 near the opening of the silo. Therefore, both 538
 494 the experimentally measured and numerically 539
 495 predicted velocity data were normalised by the 540
 496 volumetric flow rate before being compared. At 541
 497 each height above the silo opening, z , the local 542
 498 volumetric flow rate is calculated using Equa-543
 499 tion 7. The velocity components are then mul-544
 500 tiplied by the particle diameter squared and di-545
 501 vided by the local volumetric flow rate to obtain 546
 502 the normalised velocity, $\tilde{\mathbf{u}}$, where $\tilde{\mathbf{u}} = \mathbf{u}d^2/Q$. 547

503 The comparison of the vertical velocity pro-548
 504 file taken at five heights above the opening for 549
 505 the 30° silo with smooth walls (i.e. no parti-550
 506 cles attached to the wall) is shown in Figure 6, 551
 507 while the horizontal velocity profile is shown in 552
 508 Figure 7. The distance from the silo opening 553
 509 to the silo transition (the point where the cone 554
 510 becomes a cylinder) is $\approx 14.7 \text{ mm}$, hence four 555
 511 of the comparison lines are in the converging 556

conical section of the silo, while one is in the
 cylindrical section.

It is apparent that the match between the ex-
 perimentally derived and numerically predicted
 normalised velocity is good, particularly for the
 vertical velocity. The normalised velocity pre-
 dicted by the model has approximately the same
 maximum and also approximately the same cur-
 vature and shape as the MRI experimental mea-
 surements. However, the absolute velocity pre-
 dicted by the model does not match the exper-
 iment due to the discrepancy in the volumet-
 ric flow rate between the two. There is more
 noise in the horizontal measurements, and the
 prediction of normalised horizontal velocity is
 slightly worse near the silo opening, but overall
 the agreement is satisfying.

As a further test, in Figure 8 we plot the nor-
 malised vertical component of velocity along the
 axial centerline of the silo and compare the ex-
 periment to the model. It is apparent that the
 model prediction is in very good agreement with
 the experimental results.

503 3. Numerical Model Results: 50° silo

In Section III 2, the comparison of numeri-
 cal and experimental velocity fields for the 30°
 silo with smooth walls, there were no stagnant
 regions in the flow domain. The transition
 from flowing to stationary is difficult to capture
 with simple incompressible Navier-Stokes based
 models. Figures 9 and 10 show the normalised
 vertical and horizontal velocity measurements
 and predictions in the 50° silo. In this silo the
 distance from the silo opening to the transition
 point is $\approx 7.1 \text{ mm}$, hence in this case two of
 our velocity contours are in the conical section,
 while the remaining three are in the cylindrical
 section.

Remarkably, the match between experimen-
 tal and numerical model results is quite good.
 Despite the observed transition from a flowing
 to a stagnant state in the silo domain, the gran-
 ular viscosity model is able to capture the (nor-
 malised) maximum velocity, the curvature and
 shape of the velocity contours, and the approx-

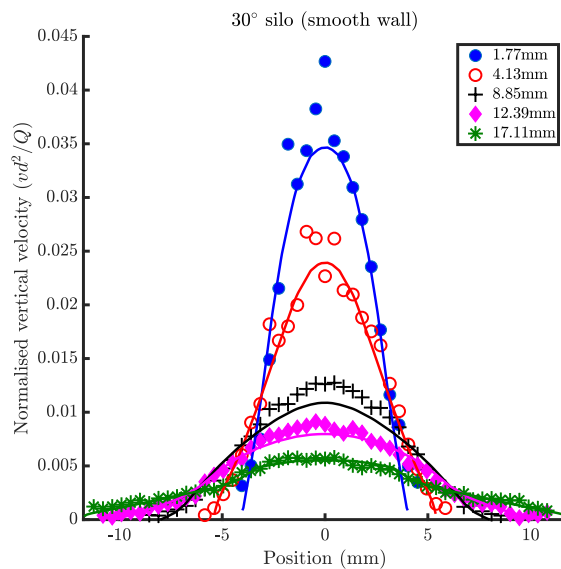


FIG. 6. The vertical velocity MRI measurements (solid circles) compared with those predicted by the numerical model (lines) for the 30° silo.

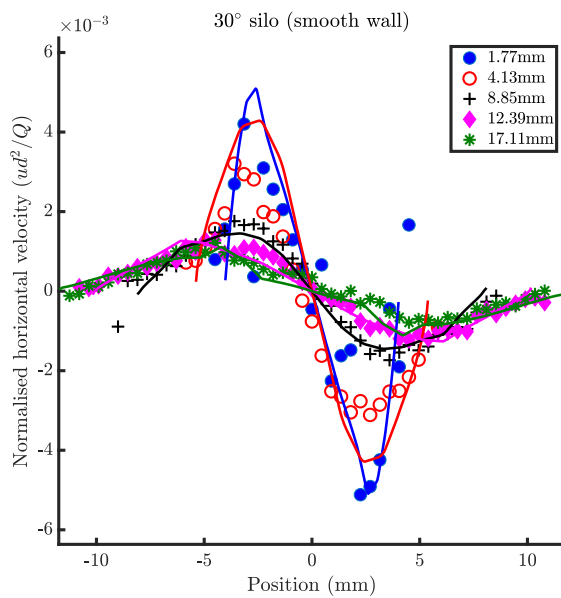


FIG. 7. The horizontal velocity MRI measurements (solid circles) compared with those predicted by the numerical model (lines) for the 30° silo, at the same locations as in the vertical velocity figure.

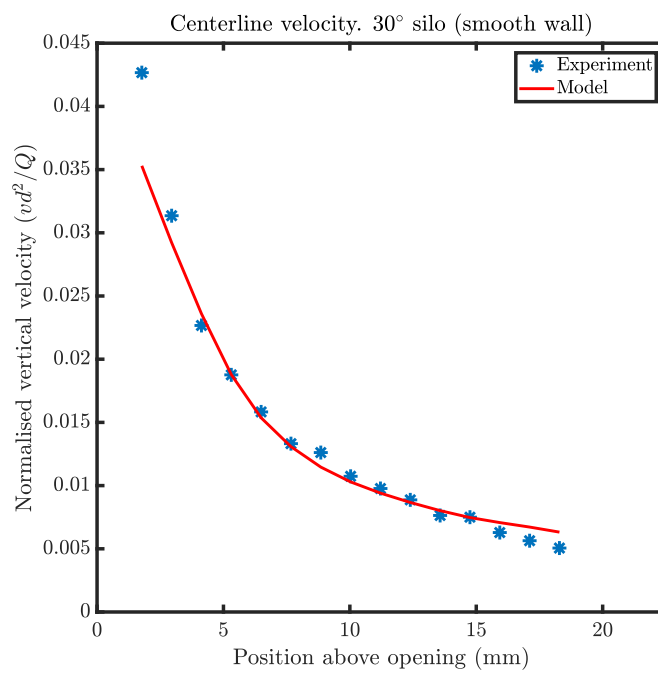


FIG. 8. A comparison of the normalised vertical velocity measured along the axial centerline of the silo compared with that predicted by the model for the 30° silo.

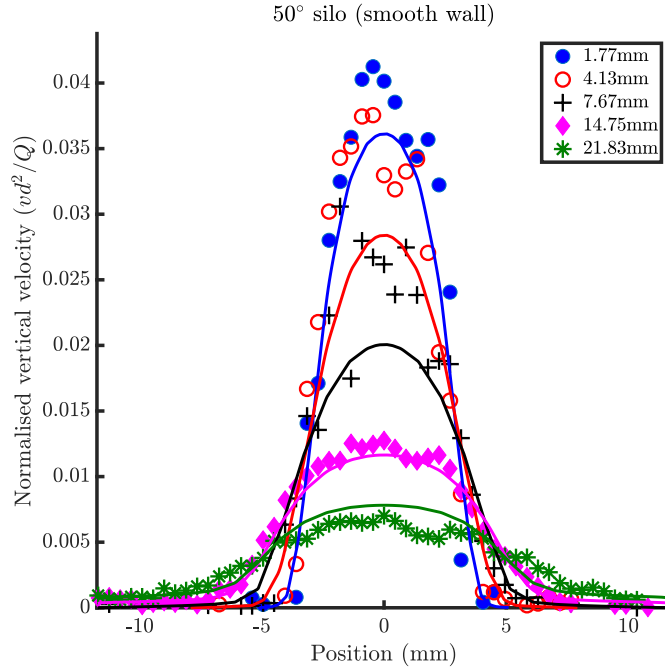


FIG. 9. The vertical velocity MRI measurements (solid circles) compared with those predicted by the numerical model (lines) for the 50° silo.

imate location of the solid/flowing boundary.

Figure 11 compares the model to experimen-
 tal normalised vertical velocity along the axial
 centerline of the 50° silo. In this case the ex-
 perimentally measured velocity contains more
 noise than in the 30° case, but it is apparent
 that the model and experiment are of similar
 and follow a somewhat similar decrease. How-
 ever, the comparison is not quite as good as in
 the 30° case.

4. Numerical Model Results: 30° silo with rough walls

The most challenging flow regime to replicate
 is the rat-holing behaviour observed in the 30°
 silo with roughened walls. In this case the ob-
 served magnitudes of horizontal velocity were
 too small to quantify since they were impercep-
 tible from the experimental noise. Hence, the

comparison of experimental to numerical pre-
 dictions was only possible for the vertical ve-
 locity component. Figure 12 displays the nor-
 malised vertical velocity profile at five heights
 above the silo opening, while Fig. 13 is the
 normalised vertical velocity measured and pre-
 dicted along the axial centerline of the silo.

It is apparent that the $\mu(I)$ model predictions
 completely fail to replicate the measured veloc-
 ity, particularly far from the silo opening. In
 the case of rat-holing flow, the $\mu(I)$ model is
 unable to capture the observed dynamics.

5. Numerical Model: Sensitivity analysis and flow rates

In order to further compare the experimental
 and numerical velocity predictions we compare
 predicted flow rates between the numerical and
 experimental results, and perform a sensitivity

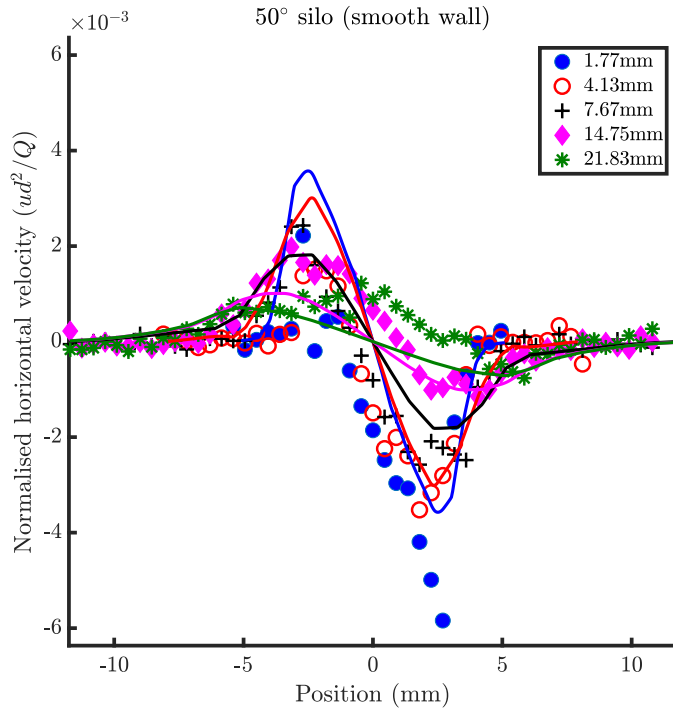


FIG. 10. The horizontal velocity MRI measurements (solid circles) compared with those predicted by the numerical model (lines) for the 50° silo, at the same locations as in the vertical velocity figure.

593 analysis on the numerical model parameters. 613
 594 To quantify the “goodness of fit” of the numerical 615
 595 predictions of velocity to the experimentally measured ones we perform linear least- 616
 596 squares regression on the normalised vertical velocity data: $\tilde{v}_{num} = b\tilde{v}_{exp}$ (i.e. we force the 617
 597 regression to pass through the origin). In the case of a perfect fit between the numerical and ex- 618
 598 perimental data, the slope of the line, b , would be unity. The normalised vertical velocity data 619
 599 at five heights above the silo opening (the same heights as used in Figures 6, 9) are combined 620
 600 and the regression is performed on the entirety of this data at once. To test the sensitivity 621
 601 of the model predictions to model parameters this process was repeated 65 times for differ- 622
 602 ent values of I_0 and μ_2 . This analysis was performed for both the 30° and 50° silos, resulting 623
 603 in 130 numerical simulations. In each simulation the value of μ_1 was kept constant at 0.6, 624
 604 while the ranges of the other two parameters were $0.05 < I_0 < 1$, and $0.9 < \mu_2 < 2.1$. In Fig- 625
 605 ure 14 the slopes resulting from the linear least-squares regression analysis are contoured for the 626
 606 30° (left) and 50° (right) silo flows respectively. The solid red dot in the contour plots indicates 627
 607 the values of the parameters used in the current work to produce Figures 6 - 13. The fine 628
 608 red line in the left plot is the contour of slope = 1 which represents a perfect fit of the numerical 629
 609 prediction of normalised vertical velocity to its experimental measurement. In general, the 630
 610 30° silo numerical simulation was better fit for lower I_0 and larger $\mu_2 - \mu_1$ values, while the 50° 631
 611 simulation had the opposite behaviour. The 30° simulation was always better fit to the experi- 632
 612 mental data than the 50° one, with reported slopes in the range 0.86 to 1.03 (by comparison, the 50° silo slopes were in the range 0.65 633
 to 0.89). For the parameters used in the main

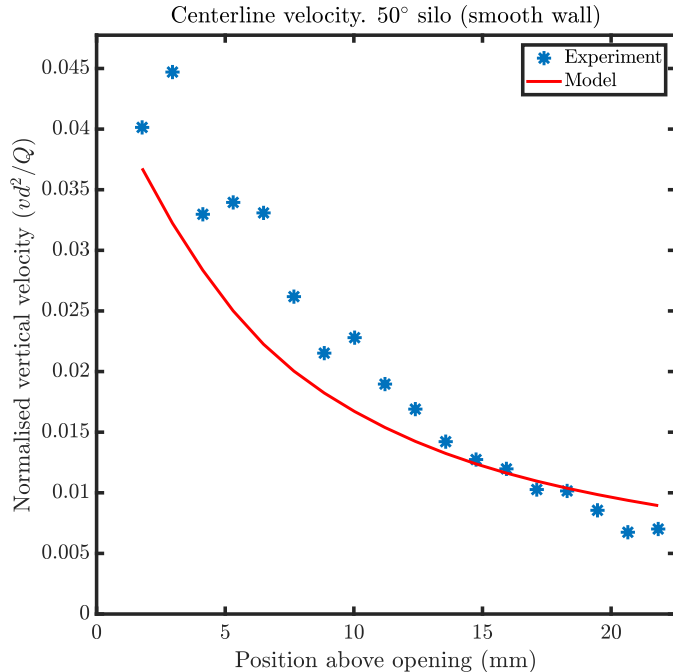


FIG. 11. A comparison of the normalised vertical velocity measured along the axial centerline of the silo compared with that predicted by the model for the 50° silo.

634 text (see Table I) the least squares slopes were 655
 635 0.94 for the 30° silo, and 0.84 for the 50° one. 656
 636 Overall, the choice of the parameters $I_0 = 0.5$ 657
 637 and $\mu_2 = 1.7$ used in this work is shown to be 658
 638 a good balance between accuracy for both the 659
 639 30° and 50° silos. 660

640 Table II presents, for each of the three silos, 661
 641 the experimentally derived mass and volumetric 662
 642 flow rates, the numerically predicted volumet- 663
 643 ric flow rate, and an approximate solids volume 664
 644 fraction in the bulk of the silo. The solids vol- 665
 645 ume fraction in the bulk was approximated by 666
 646 taking the ratio of the experimental mass and 667
 647 volumetric flow rates (in the bulk of the silo), 668
 648 then dividing by the particle density (≈ 1000
 649 kg/m^3). The predicted flowing solids fraction 669
 650 in the bulk of the 30° and 50° silos is remark-
 651 ably similar (0.46 and 0.47 respectively). How-
 652 ever, the 30° silo with particles glued to the wall 670
 653 shows a significantly lower solids volume frac- 671
 654 tion of 0.36. As previously noted, the numer- 672

ical model was of incompressible type, hence
 was not able to accurately predict the correct
 flow rate. In the table the predicted volumetric
 flow rate in the 30° silo simulation was a factor
 of ≈ 4.5 smaller than the experimentally ob-
 served one. The volumetric flow rate predicted
 in the 50° silo simulation was a lot closer to
 the experimentally observed rate, but we cau-
 tion against interpreting this as a validation of
 the model. During the sensitivity analysis the
 predicted flow rate varied by a factor of ten over
 the ranges of the parameters tested, which in-
 dicates that it is sensitive to model parameter
 choice.

IV. DISCUSSION AND CONCLUSIONS

In this work we have presented results of ex-
 perimental and numerical investigation of silo
 flow in three flow regimes; mass flow, funnel

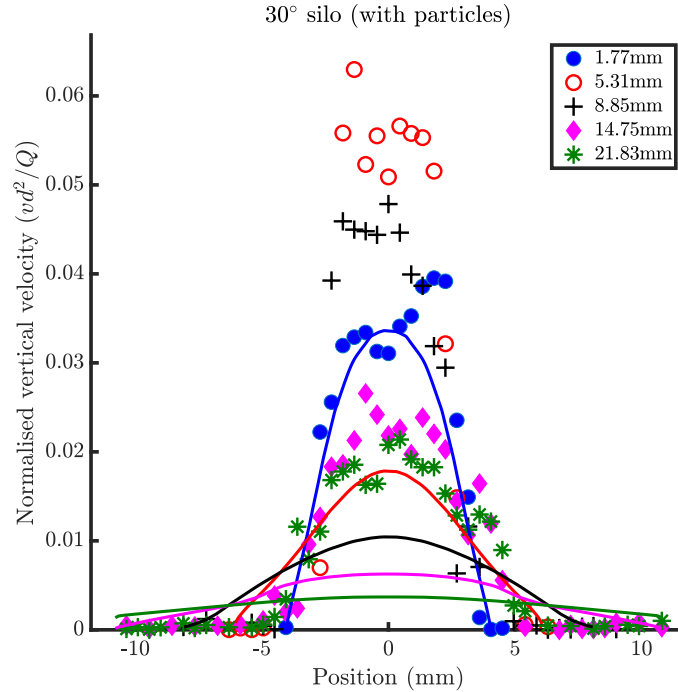


FIG. 12. The vertical velocity MRI measurements (solid circles) compared with those predicted by the numerical model (lines) for the 30° silo with roughened walls.

TABLE II: The experimentally derived and numerically predicted flow rates in the tested silos.

	\dot{m} (g/s)	Q_{exp} (bulk, cm^3/s)	Q_{num} (cm^3/s)	$\sim\phi_{exp} = (\dot{m}/Q_{exp})/\rho_p$
30°	2.11 ± 0.07	4.54 ± 0.05	0.97	0.47 ± 0.02
50°	1.74 ± 0.09	3.8 ± 0.1	4.2	0.46 ± 0.04
30° (with particles)	2.2 ± 0.1	6.1 ± 0.3	0.81	0.36 ± 0.04

673 flow, and rat-holing. Using MRI velocimetry we687
 674 measured both the horizontal and vertical com-688
 675 ponents of velocity throughout the three test689
 676 silos, including the transition from the converg-690
 677 ing conical to the cylindrical section. We found691
 678 that the 30° silo produced a mass flow, the 50°692
 679 silo produced a funnel flow, and the 30° silo with693
 680 rough walls produced a rat-holing flow. We also694
 681 presented results of a numerical model which695
 682 used the $\mu(I)$ friction law to define an effec-696
 683 tive granular viscosity for dense granular flow.697
 684 This viscosity was used to simulate the silo flows698
 685 by means of incompressible computational fluid699
 686 dynamics.

700

It was observed that the apparent volumetric flow rate in the MRI experiments was constant in the 30° silo, but was a function of height above the silo opening for the other two; the flow rate was large near the silo opening but then rapidly fell to a near constant higher in the silo. The flow rate near the opening was roughly $2\times$ that of the bulk, indicating that there is significant dilation of the flow near the silo exit opening in the 50° and 30° with rough wall cases. This is in contrast to the numerical model which enforced incompressibility of the flow. Recent studies have quantified the effect of solids fraction value at the silo opening on the

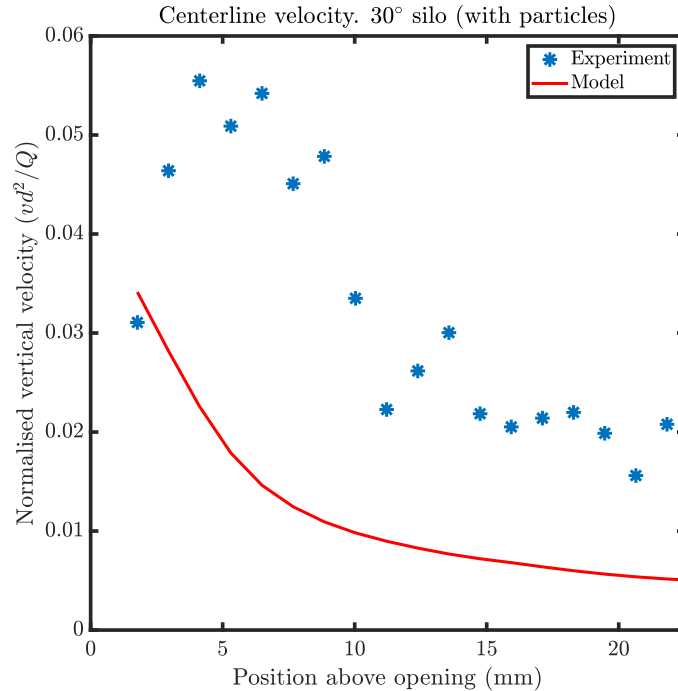


FIG. 13. A comparison of the normalised vertical velocity measured along the axial centerline of the silo compared with that predicted by the model for the 30° silo with roughened walls.

701 flow rate from the silo [54], and reported that 721
 702 solids fraction in the near opening region could 722
 703 be as low as half that in the bulk of the silo. We 723
 704 conclude that to fully capture the experimental 724
 705 measurement of the flow rate (and hence, the 725
 706 exact values of velocity) numerical models will 726
 707 likely need to include dilation effects, particu- 727
 708 larly for funnel and rat-holing flows. The ef- 728
 709 fect of dilation for the mass flow silo appeared 729
 710 negligible, but may be important to accurately 730
 711 predict the volumetric flow rate from the silo. 731

712 To allow comparison between our experimen- 732
 713 tal and numerical results, the velocity compo- 733
 714 nents of each were normalised by the local value 734
 715 of volumetric flow rate (i.e. the flow rate at 735
 716 height z above the silo opening). The resulting 736
 717 velocity fields derived from the 30° silo simu- 737
 718 lation showed excellent agreement with the ex- 738
 719 perimental data. Plots of the vertical and hor- 739
 720 izontal velocity at a series of heights above the 740

opening showed that both the shape and (nor-
 malised) maximum of the velocity contours were
 well matched, as was the vertical velocity compo-
 nent measured along the center-line of the
 silo. The comparison in the 50° silo (which
 operated in the funnel flow regime in the MRI
 experiment) were surprisingly impressive, with
 very good agreement between experimental and
 numerical results. This suggests that for appro-
 priate values of fitting parameters the $\mu(I)$ fric-
 tion law can be used to define an effective gran-
 ular viscosity for granular dynamics, even in the
 case where there are transitions from static to
 flowing regions in the domain of study.

However, for the 30° silo with roughened
 walls (which displayed rat-holing in the MRI
 experiment), the simulation results were poorly
 matched to the experimental data. The grain
 dynamics in this silo are very complicated and
 hard to capture with numerical models. Rat-

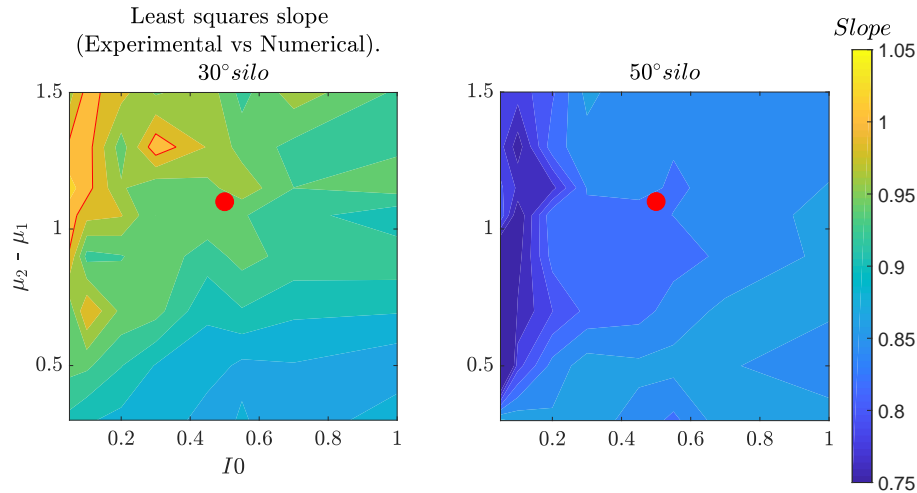


FIG. 14. Sensitivity analysis of the numerical model to parameters I_0 and $\mu_2 - \mu_1$. The contour plots display the value of the slope found by performing a least-squares linear regression between the experimental and numerical normalised vertical velocity data. The left graph is the analysis for the 30° silo and the right for the 50° one. The red dot in the plots indicated the value of the parameters used in the current work, while the fine red line in the left plot is the contour of slope = 1 (indicating a perfect fit of the numerical to experimental data).

741 holing flow in a silo is often avoided by smooth-764
 742 ing the silo walls (thus, changing the stress dis-765
 743 tribution in the silo) and/or increasing the size766
 744 of the silo opening. It is a challenge for simple767
 745 incompressible continuum visco-plastic models768
 746 of granular flow to capture these “finite particle769
 747 size” effects. Further work is needed, includ-770
 748 ing adding the effect of compressibility, to fully771
 749 capture the observed dynamics in this situation.772

750 It is clear that the $\mu(I)$ model performs admirably in a silo in the mass and funnel flow773
 751 regimes for the parameter values chosen, but774
 752 further model development is needed to fully775
 753 capture the observed phenomena in rat-holing776
 754 flow, and to accurately predict the flow rate777
 755 from the silo. Adding in a degree of compress-778
 756 ibility into the model and/or accounting for779
 757 granular non-locality and finite size effects may780
 758 improve flow rate predictions in the silo and781
 759 may help to capture more accurately flowing to782
 760 stagnant phase transitions and potentially the783
 761 rat-holing phenomenon [55]. Testing these hy-784
 762 potheses is currently being pursued by the au-785
 763

thors. Additionally, the $\mu(I)$ friction law was discovered using experimental data from relatively low friction spherical particles [56, 57]. It is unclear if the $\mu(I)$ model is the correct friction law to use for natural particles such as the poppy seeds used in this work. Furthermore, particle shape has been shown to be an important factor in the behaviour of general granular systems [58, 59], and silo systems specifically [60, 61]. Using SEM imaging we found that our poppy seeds were kidney bean shaped, and not spherical. Such an effect could be important to include in a numerical model of granular flow, although the factor does not seem critical, since we obtained very good agreement between experimental and numerical results for the 30° and 50° silos. The $\mu(I)$ parameters in the numerical model were our “best guess”. The first friction coefficient, μ_1 , was taken as the angle of repose of the poppy seeds, however, μ_2 and I_0 were chosen to be physically realistic and to try to reduce the ill-posed regions for the $\mu(I)$ model [50]. To check the dependence of model

787 results on the I_0 and μ_2 parameters a sensitiv-808
 788 ity analysis was performed. It was found that809
 789 the accuracy of the model was retained over a810
 790 wide range of parameter values, and that our811
 791 choice of I_0 and μ_2 was a good balance of ac-812
 792 curacy for both the 30° and 50° silos. To re-813
 793 duce model degrees of freedom these parameters814
 794 should be measured for the specific set of par-815
 795 ticles [62]. In addition to experimentally quan-816
 796 tifying model parameters, the development of817
 797 realistic numerical boundary conditions should818
 798 be a focus. Developing these boundary condi-
 799 tions is a significant future research challenge,819
 800 but recent work has made excellent progress to-820
 801 wards this goal [48, 49]. The observation in the821
 802 30° silo that the flow regime changes from mass822
 803 to rat-holing when the boundary condition is823
 804 changed exemplifies the necessity of accurat824
 805 boundary conditions and may indicate some-825
 806 thing more complex than a simple slip condi-826
 807 tion is needed. Finally, in recent times it has827

been shown that defining an effective granular
 viscosity using the $\mu(I)$ friction model with an
 incompressible flow assumption can be mathe-
 matically ill-posed depending on the choice of
 parameters [63]. Adding the effect of compress-
 ibility seems to alleviate this issue [50, 64]. Al-
 though we did not note any issues in our model
 for our choice of parameters, this fact serves as
 an additional motivation to transition to a com-
 pressible flow model of granular drainage from
 a silo.

The authors acknowledge the Manawatu Mi-
 croscopy Imaging Centre (MMIC) at Massey
 University for producing the SEM images of
 the poppy seeds in Figure 1. L.F. also ac-
 knowledges funding from the Royal Society
 of New Zealand (contracts RFT-MAU1501-PD
 and MAU1712). Finally, we acknowledge the
 help of Maral Mehdizad and Alex Cliff to quan-
 tify the mass flow rates in the system.

-
- 828 [1] Bruno Andreotti, Yoël Forterre, and Olivier853
 829 Pouliquen, *Granular media: between fluid and854*
 830 *solid* (Cambridge University Press, 2013). 855
- 831 [2] Ronald Midgley Nedderman, *Statics and kine-856*
 832 *matics of granular materials* (Cambridge Uni-857
 833 versity Press, 2005). 858
- 834 [3] K Kesava Rao, Prabhu R Nott, and S Sundare-859
 835 san, *An introduction to granular flow*, Vol. 10860
 836 (Cambridge University Press New York, 2008).861
- 837 [4] M Combarros Garcia, HJ Feise, S Strege, and862
 838 A Kwade, “Segregation in heaps and silos:863
 839 Comparison between experiment, simulation864
 840 and continuum model,” *Powder Technology*865
 841 **293**, 26–36 (2016). 866
- 842 [5] Thomas Weinhart, Carlos Labra, Stefan Lud-867
 843 ing, and Jin Y Ooi, “Influence of coarse-868
 844 graining parameters on the analysis of dem869
 845 simulations of silo flow,” *Powder technology*870
 846 **293**, 138–148 (2016). 871
- 847 [6] Davide Bertuola, Silvia Volpato, Paolo Canu,872
 848 and Andrea C Santomaso, “Prediction of seg-873
 849 regation in funnel and mass flow discharge,”874
 850 *Chemical Engineering Science* **150**, 16–25875
 851 (2016). 876
- 852 [7] L Staron, P-Y Lagrée, and S Popinet, “Contin-877
 uum simulation of the discharge of the granular
 silo,” *The European Physical Journal E* **37**, 5
 (2014).
- [8] Lydie Staron, P-Y Lagrée, and Stéphane
 Popinet, “The granular silo as a continuum
 plastic flow: The hour-glass vs the clepsydra,”
Physics of Fluids **24**, 103301 (2012).
- [9] Silvia Volpato, Riccardo Artoni, and Andrea C
 Santomaso, “Numerical study on the behav-
 ior of funnel flow silos with and without in-
 serts through a continuum hydrodynamic ap-
 proach,” *Chemical Engineering Research and*
Design **92**, 256–263 (2014).
- [10] Yin Wang and Jin Y Ooi, “A study of granular
 flow in a conical hopper discharge using dis-
 crete and continuum approach,” *Procedia en-
 gineering* **102**, 765–772 (2015).
- [11] Sachith Dunatunga and Ken Kamrin, “Contin-
 uum modelling and simulation of granular flows
 through their many phases,” *Journal of Fluid*
Mechanics **779**, 483–513 (2015).
- [12] Luke A Fullard, Clive E Davies, and Graeme C
 Wake, “Modelling powder mixing in mass flow
 discharge: A kinematic approach,” *Advanced*
Powder Technology **24**, 499–506 (2013).

- 878 [13] Luke Fullard, Eric Breard, Clive Davies,⁹³¹
879 Pierre-Yves Lagrée, Stéphane Popinet, and⁹³²
880 Gert Lube, “Testing the μ (i) granular rheology⁹³³
881 against experimental silo data,” in *EPJ Web of*⁹³⁴
882 *Conferences*, Vol. 140 (EDP Sciences, 2017) p.⁹³⁵
883 11002. ⁹³⁶
- 884 [14] Y Zhou, P-Y Lagrée, S Popinet, P Ruyer, and⁹³⁷
885 Pascale Aussillous, “Experiments on, and dis-⁹³⁸
886 crete and continuum simulations of, the dis-⁹³⁹
887 charge of granular media from silos with a lat-⁹⁴⁰
888 eral orifice,” *Journal of Fluid Mechanics* **829**,⁹⁴¹
889 459–485 (2017). ⁹⁴²
- 890 [15] LA Fullard, CE Davies, AC Neather, ECP⁹⁴³
891 Breard, AJR Godfrey, and G Lube, “Test-⁹⁴⁴
892 ing steady and transient velocity scalings in a⁹⁴⁵
893 silo,” *Advanced Powder Technology* **29**, 310–⁹⁴⁶
894 318 (2018). ⁹⁴⁷
- 895 [16] LA Fullard, CE Davies, G Lube, AC Neather,⁹⁴⁸
896 ECP Breard, and BJ Shepherd, “The tran-⁹⁴⁹
897 sient dynamics of dilation waves in granular⁹⁵⁰
898 phase transitions during silo discharge,” *Gran-⁹⁵¹*
899 *ular Matter* **19**, 6 (2017). ⁹⁵²
- 900 [17] Jaehyuk Choi, Arshad Kudrolli, and Martin Z⁹⁵³
901 Bazant, “Velocity profile of granular flows in-⁹⁵⁴
902 side silos and hoppers,” *Journal of Physics:*⁹⁵⁵
903 *Condensed Matter* **17**, S2533 (2005). ⁹⁵⁶
- 904 [18] A Janda, Iker Zuriguel, A Garcimartín, Luis A⁹⁵⁷
905 Pugnali, and Diego Maza, “Jamming and⁹⁵⁸
906 critical outlet size in the discharge of a two-⁹⁵⁹
907 dimensional silo,” *EPL (Europhysics Letters)*⁹⁶⁰
908 **84**, 44002 (2008). ⁹⁶¹
- 909 [19] I Sielamowicz, S Blonski, and TA Kowalewski,⁹⁶²
910 “Optical technique dpiv in measurements of⁹⁶³
911 granular material flows, part 1 of 3plane hop-⁹⁶⁴
912 pers,” *Chemical Engineering Science* **60**, 589–⁹⁶⁵
913 598 (2005). ⁹⁶⁶
- 914 [20] K Endo, K Anki Reddy, and H Katsuragi,⁹⁶⁷
915 “Obstacle-shape effect in a two-dimensional⁹⁶⁸
916 granular silo flow field,” *Physical Review Flu-⁹⁶⁹*
917 *ids* **2**, 094302 (2017). ⁹⁷⁰
- 918 [21] Selam Waktola, Andre Bieberle, Frank⁹⁷¹
919 Barthel, Martina Bieberle, Uwe Hampel,⁹⁷²
920 Krzysztof Grudziński, and Laurent Babout,⁹⁷³
921 “A new data-processing approach to study⁹⁷⁴
922 particle motion using ultrafast x-ray tomogra-⁹⁷⁵
923 phy scanner: case study of gravitational mass⁹⁷⁶
924 flow,” *Experiments in Fluids* **59**, 69 (2018). ⁹⁷⁷
- 925 [22] Krzysztof Grudziński, Maciej Niedostatkiwicz,⁹⁷⁸
926 Jerome Adrien, Eric Maire, and Laurent⁹⁷⁹
927 Babout, “Analysis of the bulk solid flow during⁹⁸⁰
928 gravitational silo emptying using x-ray and ect⁹⁸¹
929 tomography,” *Powder technology* **224**, 196–208⁹⁸²
930 (2012). ⁹⁸³
- [23] H-Y Xie and K Shinohara, “Measurement of
solids velocity in a conical hopper by mass
tracer particles,” *Chemical engineering science*
54, 455–459 (1999).
- [24] PA Langston, MS Nikitidis, U Tüzün,
DM Heyes, and NM Spyrou, “Microstructural
simulation and imaging of granular flows in
two-and three-dimensional hoppers,” *Powder
Technology* **94**, 59–72 (1997).
- [25] MS Nikitidis, U Tüzün, and NM Spyrou, “De-
termination of phase velocities in multi-phase
flows in hoppers using dual photon gamma-ray
tomography,” *Chemical Engineering Commu-
nications* **175**, 3–24 (1999).
- [26] Michail S Nikitidis, Ugur Tüzün, and
Nicholas M Spyrou, “Tomographic measure-
ments of granular flows in gases and in liquids,”
KONA Powder and Particle Journal **12**, 53–67
(1994).
- [27] Ralf Stannarius, “Magnetic resonance imaging
of granular materials,” *Review of Scientific In-
struments* **88**, 051806 (2017).
- [28] Alexander Penn, Takuya Tsuji, David O Brun-
ner, Christopher M Boyce, Klaas P Pruess-
mann, and Christoph R Müller, “Real-time
probing of granular dynamics with magnetic
resonance,” *Science Advances* **3**, e1701879
(2017).
- [29] Christopher M Boyce, Alexander Penn,
Klaas P Prüssmann, and Christoph Rüdiger
Müller, “Magnetic resonance imaging of gas-
solid fluidization with liquid bridging,” *AIChE
Journal* (2017).
- [30] CM Boyce, NP Rice, A Ozel, JF Davidson,
Andrew John Sederman, Lynn Faith Glad-
den, S Sundaresan, John Stephen Dennis, and
DJ Holland, “Magnetic resonance characteriza-
tion of coupled gas and particle dynamics in a
bubbling fluidized bed,” *Physical Review Flu-
ids* **1**, 074201 (2016).
- [31] Hilary T Fabich, Andrew J Sederman, and
Daniel J Holland, “Development of ultrafast
ute imaging for granular systems,” *Journal of
Magnetic Resonance* **273**, 113–123 (2016).
- [32] CM Boyce, A Ozel, NP Rice, GJ Rubinstein,
DJ Holland, and S Sundaresan, “Effective par-
ticle diameters for simulating fluidization of
non-spherical particles: Cfd-dem models vs.
mri measurements,” *AIChE Journal* **63**, 2555–
2568 (2017).
- [33] Hilary T Fabich, Andrew J Sederman, and
Daniel J Holland, “Study of bubble dynamics
in gas-solid fluidized beds using ultrashort echo

- time (ute) magnetic resonance imaging (mri),¹⁰³⁷
 Chemical Engineering Science **172**, 476–486¹⁰³⁸
 (2017).¹⁰³⁹
- [34] HT Fabich, TI Brox, D Clarke, JD Seymour,¹⁰⁴⁰
 SL Codd, P Galvosas, J Brown, AJ Sederman,¹⁰⁴¹
 and DJ Holland, “Measurements of the velocity¹⁰⁴²
 distribution for granular flow in a couette cell,¹⁰⁴³
 Physical Review E **98**, 062901 (2018).¹⁰⁴⁴
- [35] Toshihiro Kawaguchi, “Mri measurement of¹⁰⁴⁵
 granular flows and fluid-particle flows,” *Ad-¹⁰⁴⁶
 vanced Powder Technology* **21**, 235–241 (2010)¹⁰⁴⁷
- [36] Michael Gentzler and Gabriel I Tardos, “Mea¹⁰⁴⁸
 surement of velocity and density profiles in¹⁰⁴⁹
 discharging conical hoppers by nmr imaging,¹⁰⁵⁰
 Chemical Engineering Science **64**, 4463–4469¹⁰⁵¹
 (2009).¹⁰⁵²
- [37] ZH Gu, PC Arnold, and AG McLean, “Pre¹⁰⁵³
 diction of the flowrate of bulk solids from mass¹⁰⁵⁴
 flow bins with conical hoppers,” *Powder tech¹⁰⁵⁵
 nology* **72**, 157–166 (1992).¹⁰⁵⁶
- [38] Pierre Jop, Yoël Forterre, and Olivier¹⁰⁵⁷
 Pouliquen, “A constitutive law for dense gran¹⁰⁵⁸
 ular flows,” *Nature* **441**, 727 (2006).¹⁰⁵⁹
- [39] P-Y Lagrée, Lydie Staron, and Stéphan¹⁰⁶⁰
 Popinet, “The granular column collapse as¹⁰⁶¹
 a continuum: validity of a two-dimensional¹⁰⁶²
 navier–stokes model with a μ (i)-rheology,¹⁰⁶³
 Journal of Fluid Mechanics **686**, 378–408¹⁰⁶⁴
 (2011).¹⁰⁶⁵
- [40] Przemyslaw B Kowalczyk and Jan Drzymala,¹⁰⁶⁶
 “Physical meaning of the sauter mean diame¹⁰⁶⁷
 ter of spherical particulate matter,” *Particulat¹⁰⁶⁸
 Science and Technology* **34**, 645–647 (2016).¹⁰⁶⁹
- [41] Kiwing To, “Jamming transition in two¹⁰⁷⁰
 dimensional hoppers and silos,” *Physical Re¹⁰⁷¹
 view E* **71**, 060301 (2005).¹⁰⁷²
- [42] Nan Gui, Xingtuan Yang, Jiyuan Tu, and¹⁰⁷³
 Shengyao Jiang, “Effects of rocking frequency¹⁰⁷⁴
 and amplitude on particle discharge in rocking¹⁰⁷⁵
 bed: A dem study,” *Powder technology* **292**¹⁰⁷⁶
 31–45 (2016).¹⁰⁷⁷
- [43] Arnold McLean, “The use of standpipes fo¹⁰⁷⁸
 increasing limiting gravitational flowrate from¹⁰⁷⁹
 mass flow bins,” *KONA Powder and Partic¹⁰⁸⁰
 Journal* **11**, 139–145 (1993).¹⁰⁸¹
- [44] C Mankoc, A Janda, Roberto Arevalo, JM Pas¹⁰⁸²
 tor, Iker Zuriguel, A Garcimartín, and Dieg¹⁰⁸³
 Maza, “The flow rate of granular materials¹⁰⁸⁴
 through an orifice,” *Granular Matter* **9**, 407–¹⁰⁸⁵
 414 (2007).¹⁰⁸⁶
- [45] W Ar Beverloo, Hendrik Antonie Leniger, and¹⁰⁸⁷
 J Van de Velde, “The flow of granular solids¹⁰⁸⁸
 through orifices,” *Chemical engineering science*¹⁰⁸⁹
15, 260–269 (1961).
- [46] Paul T. Callaghan, *Translational Dynamics
 and Magnetic Resonance*, 1st ed. (Oxford Uni-
 versity Press, Oxford, 2011).
- [47] Stéphane Popinet, “Gerris: a tree-based adap-
 tive solver for the incompressible euler equa-
 tions in complex geometries,” *Journal of Com-
 putational Physics* **190**, 572–600 (2003).
- [48] Riccardo Artoni, Andrea C Santomaso, Mas-
 similiano Go, and Paolo Canu, “Scaling laws
 for the slip velocity in dense granular flows,”
Physical review letters **108**, 238002 (2012).
- [49] Riccardo Artoni and Andrea Santomaso, “Ef-
 fective wall slip in chutes and channels: ex-
 periments and discrete element simulations,”
Granular Matter **16**, 377–382 (2014).
- [50] Thomas Barker, DG Schaeffer, Michael
 Shearer, and JMNT Gray, “Well-posed con-
 tinuum equations for granular flow with com-
 pressibility and μ (i)-rheology,” *Proc. R. Soc.
 A* **473**, 20160846 (2017).
- [51] Luke Fullard and Clive Davies, “Minimising
 the spread of residence-time distribution for
 flat and heaped powders in a wedge-shaped plan-
 nar hopper,” *Particuology* **30**, 102–110 (2017).
- [52] Kenneth E Fickie, Reza Mehrabi, and Roy
 Jackson, “Density variations in a granular ma-
 terial flowing from a wedge-shaped hopper,”
AIChE journal **35**, 853–855 (1989).
- [53] RL Brown, “Minimum energy theorem for flow
 of dry granules through apertures,” *Nature*
191, 458 (1961).
- [54] Mebirika Benyamine, Pascale Aussillous, and
 Blanche Dalloz-Dubrujeaud, “Discharge flow of
 a granular media from a silo: effect of the pack-
 ing fraction and of the hopper angle,” in *EPJ
 Web of Conferences*, Vol. 140 (EDP Sciences,
 2017) p. 03043.
- [55] David L Henann and Ken Kamrin, “A predic-
 tive, size-dependent continuum model for dense
 granular flows,” *Proceedings of the National
 Academy of Sciences* **110**, 6730–6735 (2013).
- [56] GDR MiDi, “On dense granular flows,” *The
 European Physical Journal E* **14**, 341–365
 (2004).
- [57] Pierre Jop, Yoël Forterre, and Olivier
 Pouliquen, “Crucial role of sidewalls in gran-
 ular surface flows: consequences for the rheol-
 ogy,” *Journal of Fluid Mechanics* **541**, 167–192
 (2005).
- [58] Emilien Azéma, Nicolas Estrada, Itthichai
 Preechawuttipong, Jean-Yves Delenne, and
 Farhang Radjai, “Systematic description of the

- 1090 effect of particle shape on the strength proper-
 1091 ties of granular media,” in *EPJ Web of Confer-*
 1092 *ences*, Vol. 140 (EDP Sciences, 2017) p. 06026.
 1093 [59] Shiwei Zhao and Xiaowen Zhou, “Effects of
 1094 particle asphericity on the macro-and micro-
 1095 mechanical behaviors of granular assemblies,”
 1096 *Granular Matter* **19**, 38 (2017).
 1097 [60] Tamás Börzsönyi, Ellák Somfai, Balázs Szabó,
 1098 Sandra Wegner, Ahmed Ashour, and Ralf
 1099 Stannarius, “Elongated grains in a hopper,” in
 1100 *EPJ Web of Conferences*, Vol. 140 (EDP Sci-
 1101 *ences*, 2017) p. 06017.
 1102 [61] Ezequiel Goldberg, C Manuel Carlevaro, and
 1103 Luis A Pagnaloni, “Effect of grain shape on
 1104 the jamming of two-dimensional silos,” in
 1105 *EPJ Web of Conferences*, Vol. 140 (EDP Sciences,
 2017) p. 06009.
- [62] Abdoulaye Fall, Guillaume Ovarlez, David Hautemayou, Cédric Mézière, J-N Roux, and François Chevoir, “Dry granular flows: Rheological measurements of the $\mu(i)$ -rheology,” *Journal of rheology* **59**, 1065–1080 (2015).
- [63] T Barker, DG Schaeffer, P Bohorquez, and JMNT Gray, “Well-posed and ill-posed behaviour of the $\mu(i)$ -rheology for granular flow,” *Journal of Fluid Mechanics* **779**, 794–818 (2015).
- [64] Joris Heyman, R Delannay, H Tabuteau, and A Valance, “Compressibility regularizes the $\mu(i)$ -rheology for dense granular flows,” *Journal of Fluid Mechanics* **830**, 553–568 (2017).